Author(s): Kallio, Rita; Lassi, Ulla; Kauppinen, Toni; Holappa, Eveliina; Christophliemk, Mika; Luukkanen, Saija; Tanskanen, Pekka; Fabritius, Timo

Title: Leaching characteristics of Sc-enriched, Fe-depleted acidic slags

Year: 2022

Version: Published version

Minerals Engineering 189 (2022) 107901

Contents lists available at ScienceDirect

Minerals Engineering

journal homepage: www.elsevier.com/locate/mineng

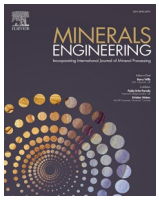

Leaching characteristics of Sc-enriched, Fe-depleted acidic slags

Rita Kallio [a,*], Ulla Lassi [b,c], Toni Kauppinen [b,c], Eveliina Holappa [a], Mika Christophliemk [b], Saija Luukkanen [a], Pekka Tanskanen [d], Timo Fabritius [d]

[a] University of Oulu, Faculty of Technology, Oulu Mining School, PO Box 3000, FI-90014, Finland
[b] University of Oulu, Faculty of Technology, Sustainable Chemistry, PO Box 3000, FI-90014, Finland
[c] Kokkola University Consortium Chydenius, University of Jyvaskyla, PO Box 567, FI-67101, Finland
[d] University of Oulu, Faculty of Technology, Process Metallurgy, PO Box 3000, FI-90014, Finland

ARTICLE INFO

Keywords:
Acidic slag
Leaching
Scandium
Sulfuric acid
Hydrogen peroxide

ABSTRACT

Scandium is currently classified as a critical raw material for the European Union, and several research projects focus on the search for new sources to supply to its expected increasing demand. The Kiviniemi mafic intrusion in Finland is a potential primary source for Sc; at Kiviniemi, Sc occurs mainly within the lattices of ferrous silicates, clinopyroxene and amphibole. Some of the main challenges in leaching of Kiviniemi-type feed material are related to either the complexity of Fe and Ti separation from Sc-containing solutions or a possible gelation problem when leaching a material with a high SiO_2 content. According to preliminary beneficiation tests, direct acid leaching of the Kiviniemi feed material was not successful mainly due to extensive leaching of Fe from the ferrous concentrate. Therefore, a processing scenario with conventional magnetic separation followed by pyrometallurgical reduction of the FeO component to tackle the Fe issue prior hydrometallurgical stage was studied in the previous parts of our project. Leaching experiments in this study focus on the possibilities to extract Sc from low-FeO, Sc_2O_3-enriched amorphous slag. Both a synthetic slag and slags produced from Kiviniemi concentrates were submitted to H_2SO_4-based leaching experiments applying dry digestion, H_2O_2-assisted leaching, and high-pressure acid leaching (HPAL). The formation of silicic acid (gelation) under acidic conditions was avoided with all these methods. With H_2O_2-assisted leaching, efficiencies reached 40–50%, whereas leaching with dry digestion was very limited. With HPAL, the leaching efficiency remained at 30–45% under experimental conditions of 2.5 M H_2SO_4, 60 bar, and 150 °C. These levels of leaching efficiencies are due to an amorphous structure and high SiO_2 content of the slag. Future options for hydrometallurgical processing of Kiviniemi-type slags could include controlled cooling of the slag to produce crystalline structures, combined potentially with further chemical modification to enable selectivity for leaching.

1. Introduction

Scandium (Sc) is currently mainly used in solid oxide fuel cells and aluminum alloys, and the prospects for using this element in advanced technology applications are highly promising (Ahmad, 2003; Duyvesteyn and Putnam, 2014; Wang et al., 2011; Zakaria and Kamarudin, 2021). Due to the very limited global annual production and market supply, Sc is currently classified as a critical element for the European Union (Blengini et al., 2020). Although classified as a rare earth element (Connelly et al., 2005), Sc behaves differently from the rest of the group due to its much smaller ionic radius, 75 pm in the octahedral coordination (Shannon, 1976). Scandium has been and currently is recovered from secondary raw materials or as a by-product from the exploitation of Ni, Ti, REE (rare earth element), Al and Zr ores (Eilu, 2017). The complexity of chemical and mineralogical composition of both primary and secondary sources of scandium reflect to the complexity of its beneficiation scenarios. Common hydrometallurgical processes for Sc extraction from various types of sources mainly involve leaching, solvent extraction, and precipitation. Although precipitation of insoluble Sc compounds from Sc-containing solutions has been mentioned as the easiest method to recover scandium (Wang et al., 2011), problems may arise from non-selective mobilization of Al, Fe and

* Corresponding author at: University of Oulu, Oulu Mining School, PO Box 3000, FI-90014, Finland.
E-mail addresses: rita.kallio@oulu.fi (R. Kallio), ulla.lassi@oulu.fi (U. Lassi), toni.kauppinen@oulu.fi (T. Kauppinen), eveliina.holappa@oulu.fi (E. Holappa), mika.christophliemk@oulu.fi (M. Christophliemk), saija.luukkanen@oulu.fi (S. Luukkanen), pekka.a.tanskanen@oulu.fi (P. Tanskanen), timo.fabritius@oulu.fi (T. Fabritius).

https://doi.org/10.1016/j.mineng.2022.107901
Received 13 July 2022; Received in revised form 27 September 2022; Accepted 16 October 2022
Available online 26 October 2022

Ti, which tend to deteriorate the purification and precipitation of suitable Sc products (Alkan et al., 2017; Borra et al., 2015; Yagmurlu et al., 2018; Zhou et al., 2018). According to a recent review of the state of the art and future prospects of scandium recovery from various sources (Botelho Junior et al., 2021), mineral acids were found to be the best leaching agents. Furthermore, as the Sc content is less than 30 ppm in most of the liquids, chelating resins were extremely recommended with solvent extractants and ionic liquids reaching over 90% of Sc separation by phosphorous group (Botelho Junior et al., 2021).

The similarity in the chemical behaviour of Sc and Fe in geological systems and in their extraction processes, which involves aqueous solutions, encourages investigations of the options offered by pyrometallurgy. The energy-intensity of pyrometallurgical processes may be compensated with the possibility to provide intermediate products, such as metallic Fe, in addition to the high value of the end-product. According to U.S.G.S. Mineral Commodity Summaries (2022), the price of Sc_2O_3 (99.99% purity) has been varying between 3800 and 4600 USD per kg in the time period of 2017–2020 with an estimate for 2021 at 2200 USD per kg, and the Sc metal price for ingot of 132–134 USD per gram, respectively. As a reference, the price of Y_2O_3 (99.99% purity) has been 3 USD per kg during the same time. Therefore, the high value of Sc combined with the complexity of Sc deportment in the feed material makes research of pyrometallurgical processing options important.

Pyrometallurgical processing provides an option to selectively separate Fe from Sc prior to hydrometallurgical processing and simplify the feed material characteristics for the extraction stage. Scandium has a high affinity to oxygen in comparison to ferrous and ferric oxides, in particular, which provides the theoretical foundation for reduction and separation of metallic products from Sc_2O_3-containing slag (Gupta and Krishnamurthy, 2005; Bisaka et al., 2017; Faris et al., 2017; Alkan et al., 2019). According to Alkan et al. (2019), a combination of pyrometallurgical and hydrometallurgical processes shows promising results for sustainable recovery of Sc from red mud. Integrated carbothermic smelting of bauxite residue followed by an acid baking and water leaching process has also been studied by Anawati and Azimi (2022). The variety of pyrometallurgical processing options for Fe oxide and REO-containing materials may include roasting, direct reduction and smelting reduction (Li et al., 2014; Faris et al., 2017). As an example, the techniques to extract Sc from the tailings of the Bayan Obo Fe-Nb-REE mine in China, with an average grade of 200 ppm Sc and main deportment in aegirine, include roasting typically with sodium hydroxide and subsequent leaching protocols with sulfuric or hydrochloric acid at temperatures on the order of 300 °C and 100 °C, respectively, (Williams-Jones and Vasyukova, 2018). Bayan Obo is the largest rare earth element resource in the world and has been beneficiated for Fe since 1927; it is currently the main producer of scandium (Jordens et al., 2013; Fan et al., 2016; Zhou et al., 2017).

It is estimated that the Kiviniemi mafic intrusion has 13.4 Mt of ferrous rock with an average Sc grade of 163 ppm. At Kiviniemi, Sc is mainly incorporated into the lattices of ferrous clinopyroxene and amphibole (Hokka and Halkoaho, 2016; Halkoaho et al., 2020; Kallio et al., 2021). In the beginning of our project, we suggested three stages of processing for Kiviniemi Sc beneficiation: 1) conventional magnetic separation of paramagnetic Sc-bearing minerals from alkali-containing diamagnetic minerals, 2) pyrometallurgical treatment of magnetic concentrate to reduce the ferrous component to metallic Fe and produce Sc_2O_3-enriched slag, and 3) hydrometallurgical processing to extract Sc from the Sc_2O_3-enriched, FeO-depleted slag. While the reduction of the FeO component from the concentrate and removal of metallic Fe can be achieved with simultaneous enrichment of the slag in Sc_2O_3 (Kallio et al., 2022a; Kallio et al., 2022b), the resulting slag also becomes enriched in SiO_2. With respect to hydrometallurgical processing, this may cause problems due to Si-gelation. However, dry digestion, acid baking and H_2O_2-assisted leaching have been mentioned as potential means to overcome the gelation problem (Voßenkaul et al., 2017; Alkan et al., 2019; Rivera et al., 2018; Kim and Azimi, 2020). Furthermore, according to Rivera et al., (2019) high-pressure acid leaching (HPAL) with H_2SO_4 at 150 °C may also provide an opportunity to extract Sc from slags. Although oxidative pressurized acid leaching has been found as an effective method for metal extraction, particularly for slags containing crystalline structures (Li et al., 2009; Perederiy, 2011; Perederiy and Papangelakis, 2017), Rivera et al. (2019) reported Sc extraction yields up to 85 wt% with HPAL of amorphous slag.

In this study, synthetic reference slag and Sc_2O_3-enriched, FeO-depleted amorphous slags produced from Kiviniemi concentrates were submitted to H_2SO_4-based leaching experiments. Dry digestion, H_2O_2-assisted leaching as well as preliminary HPAL experiments were conducted to investigate the possibilities of Sc extraction. The effects of acid concentrations, solid-to-liquid ratios and leaching temperature were investigated in more detail with H_2O_2-assisted H_2SO_4 leaching, monitoring the Sc leaching efficiency as a function of time for both synthetic reference slag and slags prepared from Kiviniemi concentrates after pyrometallurgical processing and Fe metal separation.

2. Materials and methods

2.1. Slag production

Due to the limited amount of Kiviniemi concentrates and slags produced from them (labelled as R1 and R3), synthetic reference slag sample was produced and used to test various conditions for Sc extraction in preliminary experiments. Synthetic slag with a selected composition was prepared from pure oxides (Sc_2O_3 Alfa Aesar 11217; Al_2O_3 Alfa Aesar 39814; SiO_2 Alfa Aesar 88316; CaO Alfa Aesar 33299; TiO_2 Alfa Aesar 11396; MgO Acros 263835000; MnO Alfa Aesar 11870). CaO was burned at 850 °C and stored in a desiccator. Alkalis were added as carbonates (K_2CO_3 J.T. Baker 0204 and Na_2CO_3 Merck 1.06392.0500). Chemicals were mixed and melted at 1700 °C in a platinum crucible, after which molten slag was quenched on a water-cooled copper plate to ensure the preservation of the completely amorphous structure. The produced slag was first crushed and ground to a particle size of < 125 μm, after which further grinding to $D_{90} \sim 30$ μm was conducted using a tungsten carbide vibratory disc mill.

In addition to the synthetic slag prepared for the preliminary leaching experiments, authentic slags were produced using Kiviniemi concentrates at the Process Metallurgy Research Unit, University of Oulu. Composite samples R1 and R3 included in this study represent the main Sc-bearing rock type of the Kiviniemi intrusion, medium- to coarse-grained garnet-bearing fayalite ferrodiorite and they are labelled according to the drill cores R1 and R3 they originate from (Halkoaho et al., 2020; Halkoaho and Niskanen, 2015; Kallio et al., 2021). Concentrates were prepared from crushed and ground drill core samples (P_{80} values after comminution 78 μm), which were processed as 200 g batches with a combination of low intensity magnetic separation (LIMS WD(20) 111–15) and SLon® 100 pulsating high-gradient magnetic separation (HGMS) at Metso Outotec laboratory in Pori, Finland. The concentrates produced with SLon parameters (150 rpm and 1.0 T) that had the highest Sc recovery and grade were selected for this study. Mineralogical characteristics of the concentrates used in this study are presented in more detail in Kallio et al. (2021).

The concentrates as 100 g batches were put into graphite crucibles and placed on top of a stand in an Entech high-temperature gradient furnace. The stand reached to the middle of the furnace chamber height. The graphite crucibles with a conical bottom had an inner diameter of 40 mm and an inner height of approximately 125 mm. Protective gasses enter from the bottom of the furnace alumina tube and exit from the top of the tube. Based on the total ferrous oxide content of the concentrate, graphite powder (Alfa Aesar 40797 lot: 61100109) was mixed with the concentrate in a correct proportion to ensure the complete reduction of the ferrous component. Another chemical used for modifying the slag composition was Alfa Aesar 33299 CaO (lot: P12F022), burned at 850 °C and stored in a desiccator. Addition (5%) of CaO was used to lower the

viscosity and liquidus temperature of the slag and improve the metal separation, based on previous findings in our study (Kallio et al., 2022b). At the beginning of the reduction procedure, an empty graphite crucible was weighted, after which 100 g of a mixture of concentrate + graphite + CaO was placed in the crucible applying mild compaction on the sample. The crucible was again weighed, and the tube was closed with a graphite lid which had a gas vent. Flow of a gas mixture (95% Ar and 5% CO) was switched on into the furnace with a flow rate 3 L/min and maintained throughout the heating, isotherm and cooling. The temperature program was set to start from the ambient temperature and stop at the target temperature of 1550 °C with a heating rate 5 °C/min until 1450 °C and then 2.5 °C/min until 1550 °C with 60 min for the final isotherm. After the isotherm at the target temperature, the sample was allowed to cool with the furnace until the ambient temperature and the crucible was weighed. Samples were first cut from the graphite crucible, and the large metal accumulations were removed from the bottom. The slag was cut into four pieces and taken to crushing with the Geopyörä breakage test (Bueno et al., 2021). After crushing, slag samples were ground with a tungsten carbide vibratory disc mill to the target particle size of $D_{90} \sim 30$ μm. After comminution, final magnetic separation with a hand magnet (NdFeB) was conducted to remove as much as possible residual metal inclusions from the slag.

2.2. Leaching experiments

Dry digestion experiments with concentrated H_2SO_4 (analytical reagent grade H_2SO_4 95–97 vol%, Honeywell Fluka) were conducted in an open decanter for 90 min at 75 °C using 10 g slag samples with 1:1 and 1:1.5 solid-acid ratios in the digestion stage, followed by water leaching for 30 min with S/L of 1:10.

H_2O_2-assisted H_2SO_4 leaching experiments were performed in a 0.25 L reactor immersed in a silicon oil bath. The reactor was closed using a reflux condenser to prevent any volatilization during leaching. Selected process variables for the leaching (acid concentration, temperature, time, S/L ratio) were investigated first to optimize the Sc yield with a synthetic slag (Table 1). In all our experiments, the agitation speed was maintained at 375 rpm using a magnetic stirrer. The total leaching time was 90 min. During the first experiments focusing on acid concentration, the S/L ratio was maintained at 1:10 and the experimental temperature was kept at 100 °C.

The leaching experiments were conducted using 5.00 ± 0.005 g of slags. The slag was placed in the reactor, after which sulfuric acid was added, followed by H_2O_2, and the timing of the leaching commenced. During the experiment, temperature of the slurry was monitored prior to each sampling, which was made at 15, 30, 60 and 90 min. Samples (3.3 mL) from the slurry were withdrawn and syringe filtered with a Fisher Brand 25 mm PTFE hydrophilic 0.45-μm syringe filter, after which the obtained liquids were diluted 10-fold with Milli-Q water prior to sending them for analysis with ICP-OES. After the final sampling at 90 min, the remaining slurry was first filtrated with a Buchner vacuum filter using Munktell (Ahlstrom) paper (quality 1001, 2–3 μm, 1200 s) and the final filtration with a PTFE hydrophilic 0.45-μm syringe filter. Solids were dried in oven overnight at 60 °C. The remaining undiluted liquid was cold-stored. Selected filtrated solid residues were analyzed with ICP-OES at the Eurofins Ahma laboratory in Oulu, while liquids were analyzed with ICP-OES at the University of Oulu. The analytical procedures of sample characterization are described in more detail in the following section.

Table 1
Selected H_2O_2 + H_2SO_4 leaching conditions and studied variables for factorial design with the synthetic slag.

Factor	Level −1	Level 0	Level + 1
H_2SO_4 molarity	1.5	2.5	3.5
H_2O_2 molarity	1.5	1.5	1.5
H_2O_2 molarity	2.5	2.5	2.5
H_2O_2 molarity	3.5	3.5	3.5
Solid-to-liquid ratio	1:5	1:10	1:20
Acid molarity	2.5 + 2.5	2.5 + 2.5	2.5 + 2.5
Temperature (T °C)	50	75	100
Acid molarity	2.5 + 2.5	2.5 + 2.5	2.5 + 2.5

Pressurized leaching experiments were performed in a Hastelloy C22 stainless-steel reactor (Parr, Moline, IL, USA) equipped with a cylindrical HASTELLOY®C-267 alloy autoclave (300 mL). The reactor was connected to a temperature and mixing controlling unit. The reaction temperature was kept constant at 150 °C with a precision of ±1 °C. The reactor was loaded with 140 mL of leaching solution (2.5 M H_2SO_4 prepared from analytical reagent grade H_2SO_4 95–97 vol%, Honeywell Fluka) and 7.000 ± 0.002 g of slag with S/L being 1:20. The suspension was stirred at ca. 375 rpm. The measurement of the retention time was started when the set reaction temperature was achieved with a total duration of 90 min. Samples (4 mL) were collected directly after the experiment from the hot solutions by filtering out solids with a 0.45-μm filter on a Buchner funnel. Following the filtration, the residues were dried at 60 °C overnight and sent for chemical analysis (ICP-OES) and XRD. The air pressure was increased from 0 to 10 bar and 60 bar while the temperature was maintained at 150 °C for each experiment. Three experiments were conducted on the synthetic slag and one for slag R3.

The leaching efficiency (η*i*) for metal extraction can be calculated in a variety of ways; for the purpose of this study, the following equation was applied (Zhou et al., 2018):

$$\eta i = \frac{ciV}{mxi} * 100\% \quad (1)$$

where c_i is the metal concentration in the leaching solution; V is the volume of the leaching solution, m is the mass of the slag; and x_i is the mass fraction of the metal element in the slag. For comparison, solid residues from some experiments were also analyzed with ICP-OES to calculate the yield with the following equation:

$$X = \left(1 - \left(\frac{Cr}{Co}\right)\right) * 100\% \quad (2)$$

where C_r and C_o is the scandium content in the residue and in the original slag, respectively.

2.3. Characterization

Particle size distributions were determined with Anton Paar PSA (Particle Size Analyzer) 1190 LD (Laser Diffraction) in liquid measurement mode with ultrasound duration of 60 s. Water was used as the carrier liquid without dispersing agents; satisfactory dispersion was obtained via ultrasound. The obscuration target values were between 5% and 30%.

Carbon and sulfur analyses were conducted with a LECO CS 200 Carbon and Sulfur Analyzer. Geostats Mining Industry Consultants Reference Material Manufacture and Sales Certified Reference Material GGC-07 (C = 0.56%, S = 0.51%) was used as a calibration standard. The analytical method C 0.5 – S 0.5 with an analysis time of 40 s was applied. Iron Chip accelerator + Lecocell Combustion accelerator was used as the blank sample. The accuracy of the results is 0.01% for C and 0.005% for S.

X-ray diffraction (XRD) was utilized to detect whether any crystalline phases were present in the used slags and characterize the residues after leaching experiments. Spectra were recorded using a Rigaku SmartLab 9 kW XRD diffractometer with Co/Kα radiation at 40 kV and 135 mA. The speed of data acquisition was 4°/min with 0.02°/steps and 2θ range of 10-130°. Data processing was performed with PDXL2 software and PDF-4 2022 database.

For analyzing slags and leaching experiment residues, a JEOL JXA-8530FPlus electron probe microanalyzer (EPMA) was used at the Centre for Material Analysis (CMA), University of Oulu. Analyses were

carried out on polished, carbon-coated blocks. The analyses were performed with an accelerating voltage of 15 kV, a beam current of 15nA, and a beam diameter of 1–5 μm. Data on detection limits and the standards are provided as electronic Supplementary Data (Table S1).

Residues after leaching experiments were also characterized with a JEOL JSM-7900F field emission scanning electron microscope (FESEM) equipped with an Oxford Instruments Ultim Max 65 energy-dispersive (EDS) detector and Aztec Mineral software at the CMA. A small amount of residue powder was placed on a carbon tape, after which samples were coated with carbon. Secondary electron images with X-ray mapping and point analyses were conducted with an accelerating voltage of 15 kV, a probe current of 5nA and a working distance of 10 mm.

The ICP-OES determinations of Al, Ca, Fe, K, Mg, Mn, Na, Sc, Si and Ti in 10-fold diluted solutions were carried out with an Agilent 5110 VDV ICP-OES instrument. The analytical results are given as mean values of 5 replicate measurements. Yttrium (wavelength 371.029 nm) was used as an internal standard to correct for the sensitivity drift and matrix effects in the measurements. The calibration standards for the ICP-OES analyses were prepared by diluting from 1000 mg/L single-element standards. 2% nitric acid (Honeywell Fluka, puriss. p.a., ACS reagent, ≥69%) was added to each calibration standard. Quality control standard samples and blank samples were analyzed for quality assurance purposes. For each sample, 10-, 40- and 200-fold dilutions were prepared with 2% nitric acid. The results of Al, Ca and Ti were taken from the 200-fold diluted samples, those of Mg and Na from the 40-fold diluted samples and for the rest of the components, 10-fold diluted samples were used. Emission lines used in the ICP-OES measurements (Table S2) and elemental concentrations of the calibration standards (Table S3) are provided in electronic supplementary data.

For ICP-OES analysis at Eurofins Ahma, the prepared bulk samples of solid leach residue and slag (0.2 g) were fused with anhydrous sodium peroxide in a zirconium crucible by heating in an electric furnace at 700 °C for one hour. The melt was dissolved in hydrochloric acid. The final solution was diluted with water prior to instrumental analysis. A routine method was used in which 27 elements were measured with an ICP-OES Thermo Electron ICAP 6500 Duo instrument.

3. Results and discussion

3.1. Slag characteristics

Fig. 1A-E present a set of images from Kiviniemi slag R1 before final grinding; As can be seen from the stereomicroscope image Fig. 1E, slag particles contain occasional black inclusions, which are metal droplets remained in the slag despite slag modification and experimental final temperature of 1550 °C, at which the isotherm was 60 min. Although most of the metal is segregated into large accumulate at the bottom (Fig. 1D), further magnetic separation is still required after grinding and prior to hydrometallurgical processing. Fig. 2 presents diffractograms of slag R1 after magnetic separation of the ground slag, according to which the slag submitted to hydrometallurgical experiments can be considered amorphous. Diffractograms for the synthetic slag and slag R3 are presented in the electronic supplementary material (Figure S1).

Images of Kiviniemi slag R3 are shown in Fig. 3. As illustrated by the stereomicroscopic image in Fig. 3A, similar black metal inclusions occur in slag particles as in slag R1. Fig. 3B confirms that despite the improvement in metal separation accomplished via slag modification, there remains occasional larger (100–150 μm) metal inclusions in the slag in addition to sporadic, very small (<5 μm) droplets. A close-up image in Fig. 3C demonstrates a homogeneous area without visible metal inclusions or any crystalline structures in the slag, while Fig. 3D provides details and the structure of a metal inclusion consisting of ferrite and steadite Fe_3P (bright white), graphite (black) and titanium carbide (TiC) (medium gray) at the contact between slag and metal, as confirmed by EPMA analyses.

In terms of the main components, the biggest difference between the synthetic slag and slags produced from Kiviniemi R1 and R3 concentrates is in their Ca content (Table 2); the synthetic slag composition was originally calculated to represent FeO-depleted slag without any modification. However, along the progression of our study, a moderate CaO addition was used to improve the reduction of the FeO component and metal separation from the slag, and therefore slags produced from Kiviniemi concentrates R1 and R3 are higher in Ca. Synthetic slag also has slightly higher Al content. Carbon and S contents, as determined with LECO, are presented in Table 3. Despite performing similar processing for both the R1 and R3 slags, the carbon content R1 is higher than in R3. On the contrary, the sulfur content is slightly higher in R3, with LECO providing even higher contents for R3 than ICP-OES. The higher amount of carbon in R1 indicates that some amount of material from the graphite crucible remained in the slag.

Cumulative particle size distributions of the slag samples, as determined with the laser diffraction method, are given in Fig. 4, showing the relative number of particles at or below a particular size. The target of grinding and desired particle sizes for all three slags was at $D_{90} \sim 30$ μm, which was accomplished for the synthetic and slag R3 with D_{90} of 26 and 30 μm, respectively, whereas R1 remained slightly coarser with a D_{90} value of 34 μm.

3.2. Atmospheric leaching of synthetic slag

A few experiments with the synthetic slag were conducted in the beginning with dry digestion procedures, but due to the very low Sc extraction (≤22 mg L^{-1} after 90 min leaching), the decision to focus on H_2O_2-assisted H_2SO_4 leaching was made. First, the effects of H_2O_2 molarity at various levels of H_2SO_4 molarity were investigated at 100 °C and S/L of 1:10. Based on the results (Fig. 5), the efficiency of leaching at various H_2SO_4 molarity levels is highest when the molarities of both H_2SO_4 and H_2O_2 are at the same level. Furthermore, the highest efficiency is achieved with the highest molarities of 3.5 M H_2SO_4 and 3.5 M H_2O_2. Increasing the H_2O_2 molarity at the 1.5 M H_2SO_4 level decreases the leaching efficiency. On the other hand, with 1.5 M H_2O_2, there is

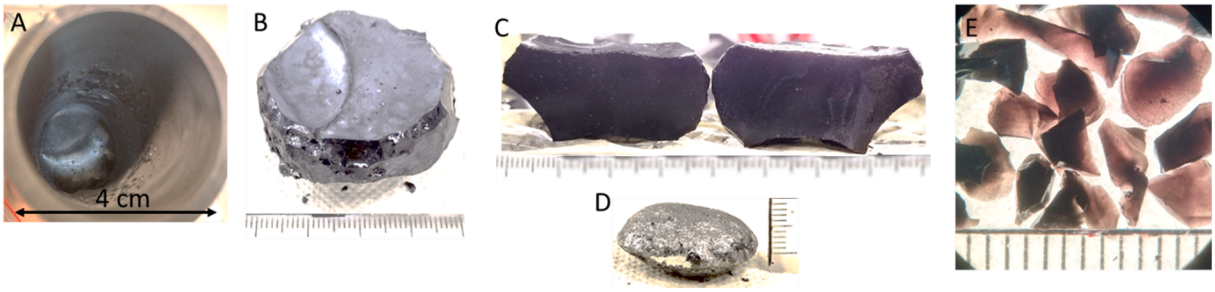

Fig. 1. Set of images from Kiviniemi slag R1 before final grinding. (A) Slag in a graphite crucible after reduction; (B) slag cut from the crucible; (C) cross-section of the slag; (D) large metal accumulation, (E) stereomicroscope image of crushed slag particles.

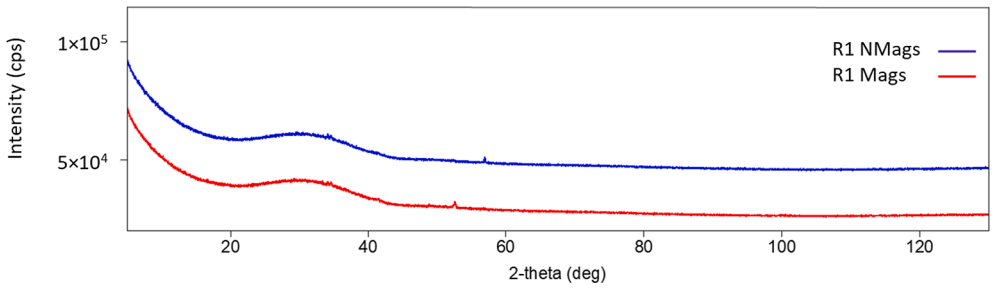

Fig. 2. XRD patterns for slag R1 after grinding and magnetic separation for both magnetic (Mags) and Non-Magnetic (NMags) fractions.

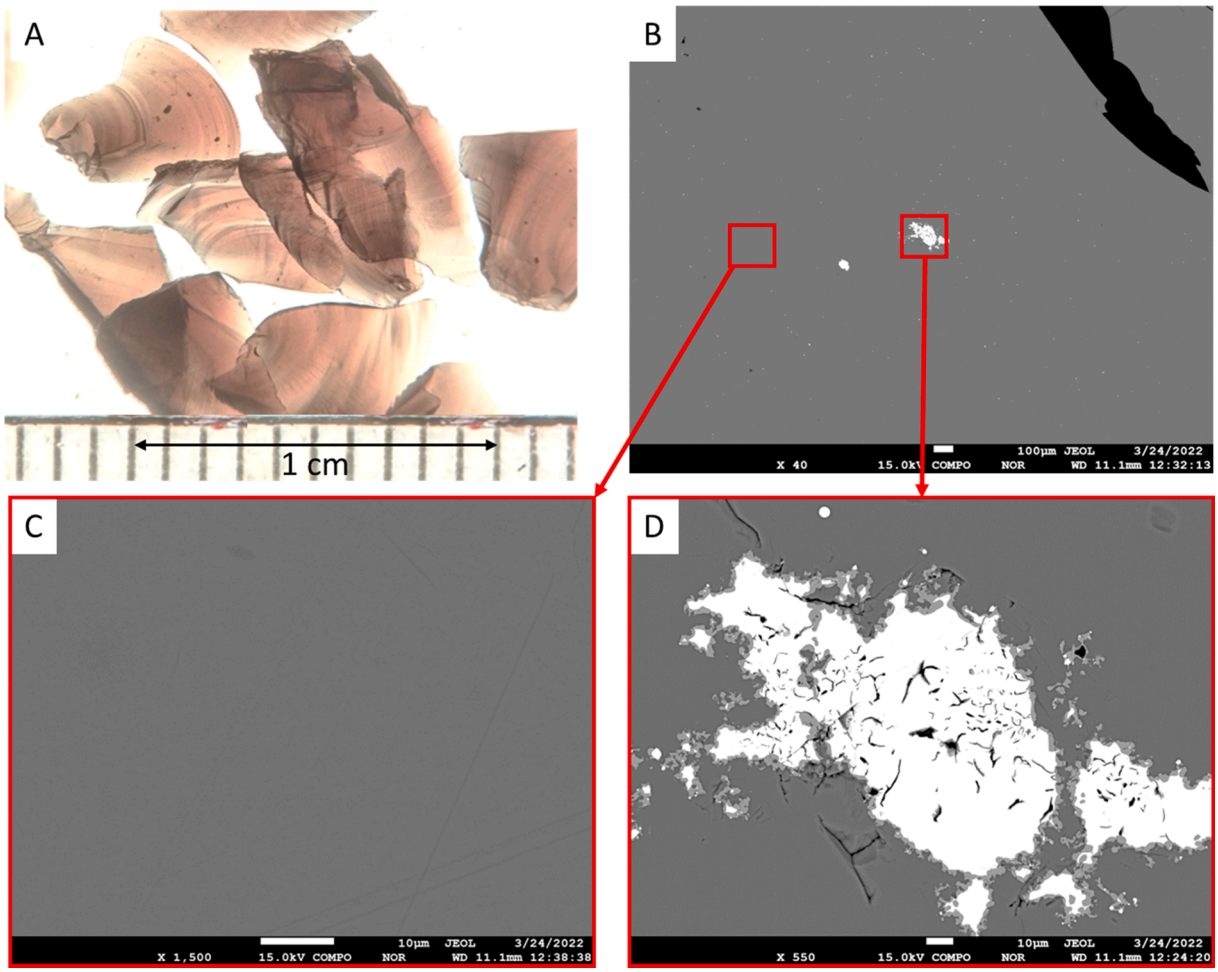

Fig. 3. Images of Kiviniemi slag R3 before grinding. **(A)** Stereomicroscope image of crushed slag particles; **(B)** back-scattered electron image of slag with occasional larger (100–150 µm) metal inclusions; **(C)** close-up view of homogeneous slag without visible metal inclusions; **(D)** close-up view of a larger metal inclusion, in which the brightest phase is ferrite with steadite and intermediate grey at the contact between metal and slag is titanium carbide.

Table 2
ICP-OES-based chemical compositions (wt%) of Sc slags used in leaching experiments.

	Al %	Ca %	Fe %	K %	Mg %	Mn %	P %	S %	Sc %	Si %	Ti %
Synthetic slag	8.13	8.21	0.05	1.34	0.97	0.70	<0.05	<0.02	0.611	26.30	2.09
R1	6.27	13.80	0.06	1.68	1.68	0.60	<0.02	0.27	0.031	24.70	2.66
R3	7.40	12.35	0.05	1.69	0.86	0.51	<0.02	0.29	0.039	25.95	1.99

only little improvement with increasing H_2SO_4 molarity. Throughout the experiments both with the synthetic and Kiviniemi slags, the temperature of the slurry remained within ± 2 °C from the target temperature.

Effects of temperature and the S/L ratio on the leaching efficiencies are presented in Fig. 6A and 6B; temperature effects were investigated with S/L of 1:10 and effects of varying S/L (1:5, 1:10 and 1:20) were investigated at 100 °C. Based on these results, temperature has a strong

Table 3
Carbon and sulfur contents (wt%) of Kiviniemi slags R1 and R3 as measured with LECO S200.

Sample	mass, g	C%	S%
R1	0.0197	0.162	0.281
R1	0.0187	0.164	0.278
Blank	1	0.000867	0.00047
R3	0.0249	0.0289	0.3485
R3	0.0267	0.0292	0.3505
Blank	1	−0.00075	−0.00101

effect on improving the leaching efficiency: at 50 °C, it reaches a maximum of 29% after 90 min of leaching, while at 100 °C, it reaches 40% after the same leaching time. With respect to S/L ratios, the leaching efficiencies increase to 51% with S/L of 1:20 after 90 min of leaching.

In all leaching experiments, as soon as H_2O_2 was added into the reactor, formation of an orange complex was observed. This is due to the combined effects of H_2SO_4 and H_2O_2, which contribute to the soluble titanium peroxosulfate formation during leaching. According to Alkan et al. (2018), the formation of soluble titanium peroxosulfate and the mechanism of dissolution in pregnant leach solution (PLS) can be described via the following chemical reactions:

$$TiO_2 + H_2SO_4 \rightarrow [TiO]SO_4 + H_2O \quad (3)$$

$$[TiO]SO_4 + H_2O_2 \rightarrow [TiO\text{-}O]SO_4 + H_2O \quad (4)$$

where titanium oxide reacts first with sulfuric acid to produce oxotitanium sulfate and water. Formation of orange-yellow $[TiO\text{-}O]SO_4$ complex was observed in all leaching experiments. Fig. 7 exhibits photographs of diluted samples taken at 15, 30, 60 and 90 min after leaching of the synthetic slag with 3.5 M H_2SO_4 + 3.5 M H_2O_2 at 100 °C and S/L of 1:10. Also an undiluted residual liquid is shown on the right. As can be seen, the color of the diluted sample is not as strong after the 90 min leaching experiment, which is most likely due to decomposition of the peroxide in the complex, leaving titanium (IV) in a less coloured or eventually even colourless solution.

The secondary electron images in Fig. 8 with corresponding X-ray elemental maps for Si, Ca, Al and S visualize the characteristics of the synthetic slag leach residues. The images exhibit intact larger slag particles and smaller particles with varying composition. Calcium sulfates were occasionally detected in the electron microscopy investigations, but the residue exhibits a mixture of unreacted and reacted slag particles with areas on the surfaces that are enriched in sulfur. Silica-enriched small particles were commonly observed among the finest particles of the residue (Fig. 8B) and on the surfaces of larger particles. Silica precipitation with a crystalline structure has been suggested as a mechanism in avoiding silica gel formation (Alkan et al., 2018), but according to the XRD patterns of our experiments (Figure S2), residues after H_2O_2-assisted H_2SO_4 leaching did not contain crystalline SiO_2.

The back-scattered electron image of the synthetic slag leach residue (2.5 M H_2O_2 + 2.5 M H_2SO_4, S/L 1:10, T = 100 °C) in Fig. 9 shows a mixture of intact slag particles with hydrolyzed, silica-enriched particles and zoned particles (darker grey color in the image), with original slag composition preserved in the middle. Examples of compositions of particles determined by EPMA are presented in Table 4; the darker particles consist of SiO_2 with low analytical totals, which is an indication of the presence of undetectable hydroxyl with electron microprobe. Darker particles and darker zones are depleted from other components. Summary of binary plots of CaO, Al_2O_3, TiO_2 and Sc_2O_3 with SiO_2 (wt%) from slag particles prior to and after leaching are provided in electronic supplementary data (Figure S3).

3.3. Atmospheric leaching of Kiviniemi R1 and R3 slags

Based on the results with the synthetic slag, two levels of acid molarities, 2.5 M H_2SO_4 + 2.5 M H_2O_2 and 3.5 M H_2SO_4 + 3.5 M H_2O_2, were selected and used for the Kiviniemi slags R1 and R3 at 100 °C. Furthermore, two levels of S/L (1:10 and 1:20) were also included, thus forming a total of 4 different molarity-S/L combinations. With the Kiviniemi slags, duplicate experiments were conducted to provide an estimate of the variability of the results. Leaching efficiencies of Sc as a function of leaching time (15–90 min) are presented in Fig. 10. It reveals that there is a significant difference in the leaching characteristics of these two slags. The Sc leaching efficiency of slag R1 is systematically significantly lower than that of slag R3. Decreasing S/L improves the Sc leaching efficiency for both slags, as is also observed for the synthetic slag. Although very close to the target value, the slightly coarser particle size range in R1 is considered the main reason for the lower leaching efficiency as compared to the synthetic slag and slag R3.

Leaching efficiencies for all elements analyzed from the solutions after 90 min leaching are displayed in Fig. 11. This summary includes leaching efficiency data at both molarity levels (2.5 M and 3.5 M for both H_2SO_4 and H_2O_2) and at both S/L ratios (1:10 and 1:20) that were tested. All other elements show very similar leaching efficiencies, except silicon. Furthermore, the leaching efficiency for all elements with slag R1 is consistently lower compared to slag R3 due to the aforementioned reason. Based on the ICP-OES results from the solid residues, the leaching efficiencies of Sc for R1 and R3 after 2.5 M H_2SO_4 + 2.5 M H_2O_2 leaching with S/L 1:20 at 100 °C were 12.8 and 37.2%, respectively, which is in line with the results calculated based on liquid compositions (Fig. 10A and 11).

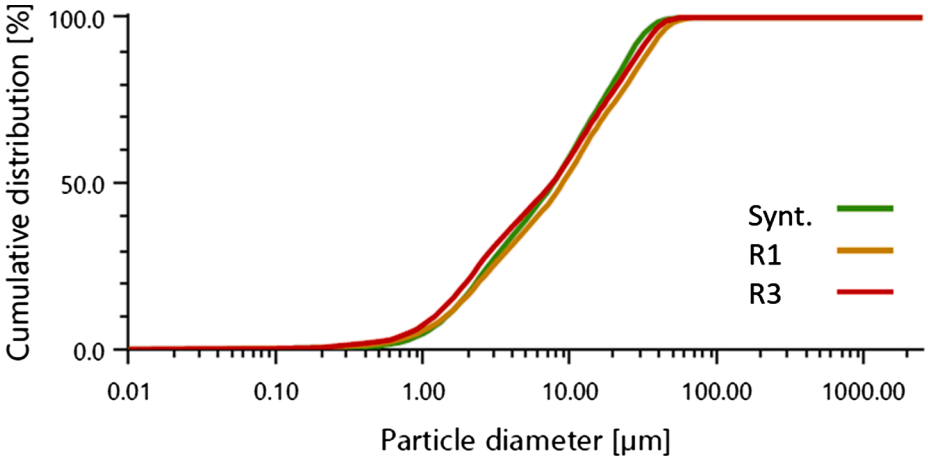

Fig. 4. Cumulative particle size distributions determined with PSA 1190 LD for the synthetic slag and Kiviniemi slags R1 and R3.

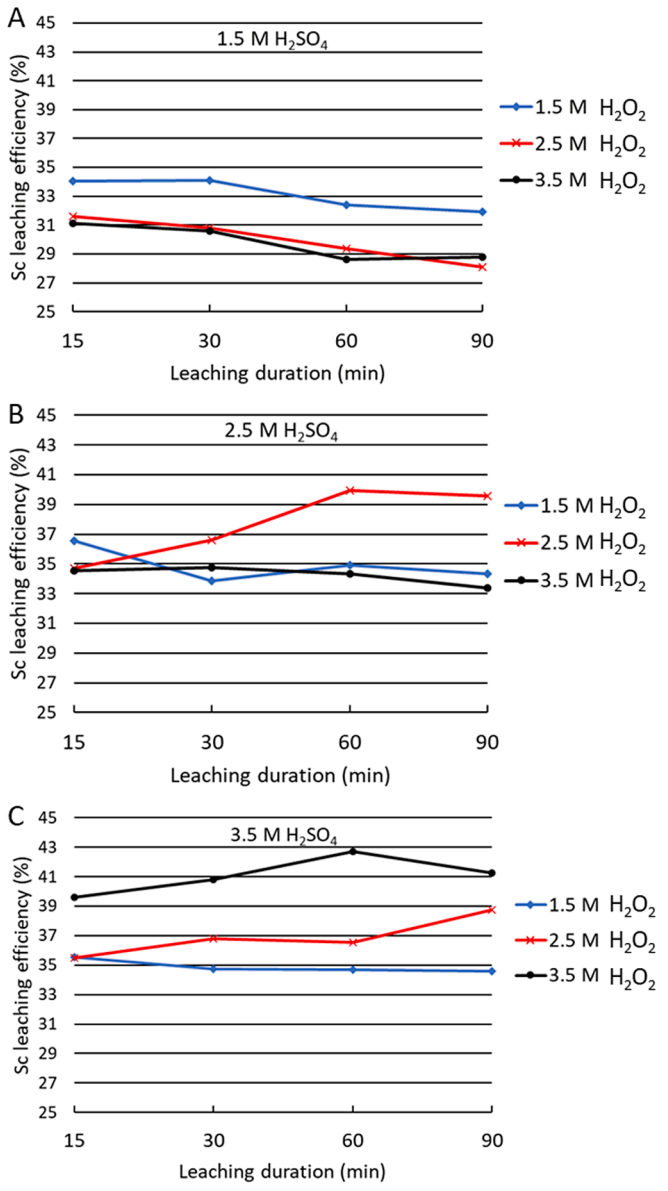

Fig. 5. Effects of H_2O_2 and H_2SO_4 molarity on Sc leaching efficiency for synthetic slag as a function of H_2O_2 molarities together with **(A)** 1.5 M H_2SO_4; **(B)** 2.5 M H_2SO_4 and **(C)** 3.5 M H_2SO_4.

The secondary electron image with corresponding X-ray elemental maps for Si and Ca shown in Fig. 12 visualize the characteristics of the slag R3 leach residues. EDS analysis points are also presented, with the results listed in Table 5. Although the analytical results by EDS on unpolished surfaces and particularly for particles smaller than 5 μm can be considered indicative only, element maps combined with the chemical data in Table 5 indicate the presence of small silica-containing particles depleted from other slag components.

A back-scattered electron image of the slag R3 leach residue is presented in Fig. 13 and the corresponding results of EPMA point analyses representing the center of the particles are shown in Table 6. Unlike with the synthetic slag, there were not larger, easily detectable, silica-enriched hydrated particles in the residue. Although the R1 and R3 slag particles exhibit similar changes along the cracks and on the edges of the particles as synthetic slag, these areas are too small to be analyzed with EPMA. However, the presence of smaller silica-enriched particles occurring as agglomerates or on the surfaces of larger particles (Fig. 12) are interpreted to represent essentially small slag particles from which other elements have been extracted, leaving a siliceous residue. This is possibly accompanied with agglomerates of polymerized silica; silica precipitation under very acidic conditions has been described to proceed via fast polymerization of monomeric silica from solution, which then flocculate (Gorrepati et al., 2010; Voßenkaul et al., 2017).

The challenges related to leaching of Kiviniemi-type slags include the extremely high silica content (53–56 wt% SiO_2) as compared to the data reported in the literature on hydrometallurgical processing of various slags (Alkan et al., 2019; Kim and Azimi, 2020; Perederiy, 2011; Rivera et al., 2019; Yagmurlu et al., 2019). Silica gel formation is one of the most common problems at lower temperatures in hydrometallurgical processing of silica-containing resources, such as bauxite residues, which have SiO_2 contents in the range of 3.0–23.8 wt%, or acidic slags derived from processing of bauxite residues with SiO_2 38 wt% (Alkan et al., 2019, Yagmurlu et al., 2019). Therefore, for materials with SiO_2 contents ranging 53–56 wt%, the suppression of silica gel formation was one of the focus points in these experiments. Soluble silica is found as monomeric orthosilicic acid, $Si(OH)_4$, in acidic conditions (pH < 7)

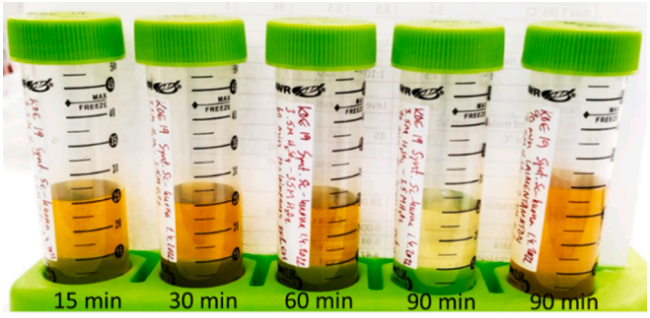

Fig. 7. Diluted (10x) 15-, 30-, 60- and 90-min samples after leaching synthetic slag with 3.5 M H_2SO_4 + 3.5 M H_2O_2 at 100 °C and S/L of 1:10. A sample of undiluted residual liquid is shown on the right.

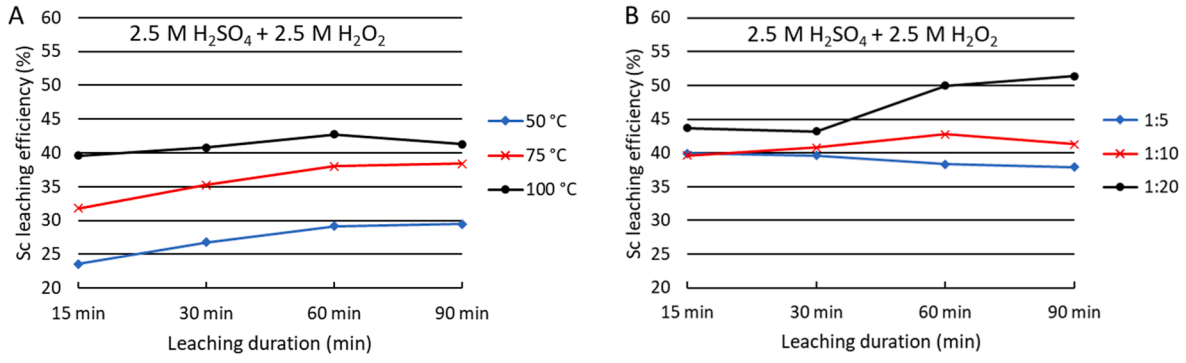

Fig. 6. Effects of **(A)** temperature (S/L = 1:10) and **(B)** S/L (T = 100 °C) on leaching efficiency of Sc for synthetic slag with 2.5 M H_2SO_4 and 2.5 M H_2O_2.

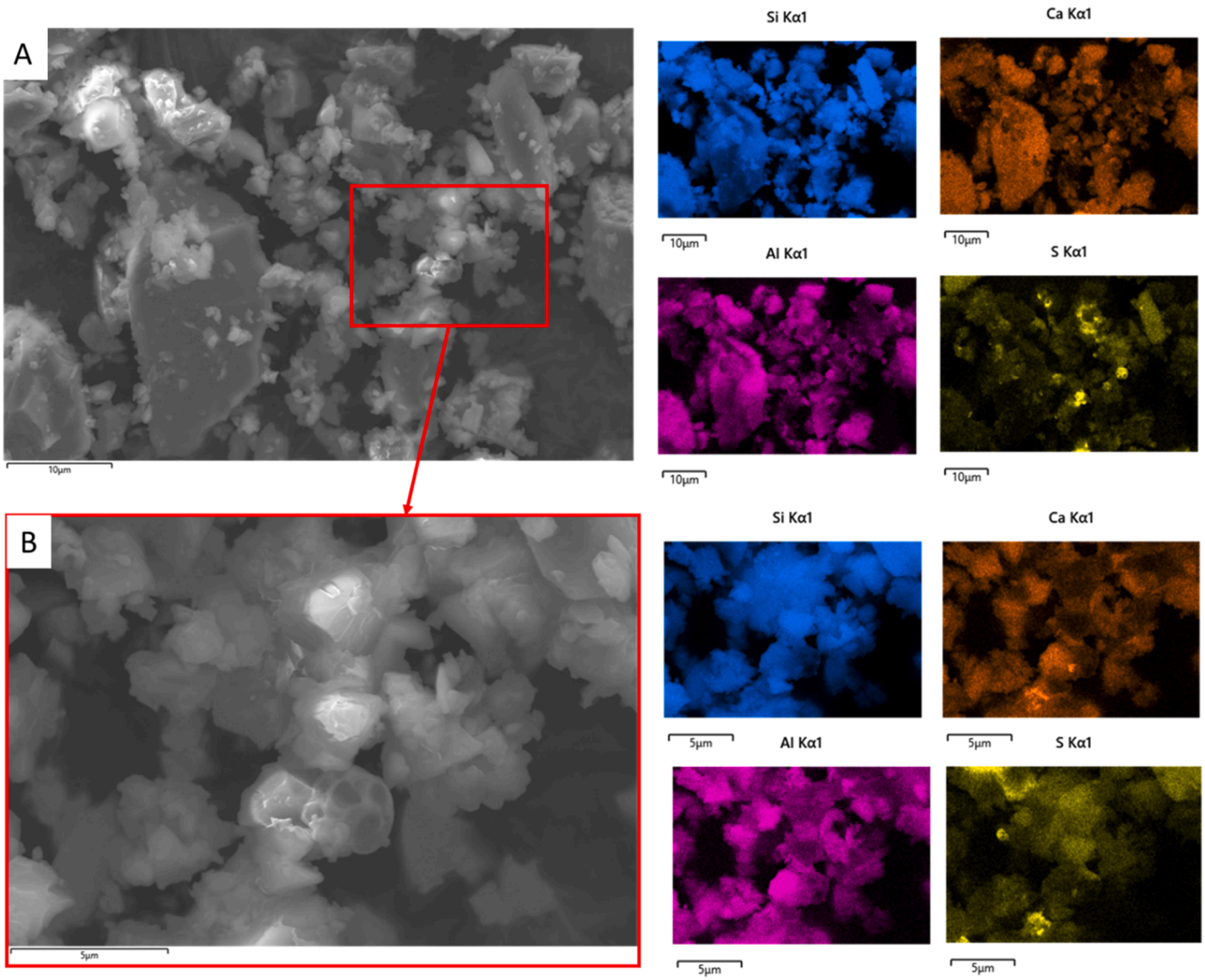

Fig. 8. **(A)** Secondary electron image of synthetic slag leach residue (2.5 M H_2O_2 + 2.5 M H_2SO_4, S/L 1:10, T = 100 °C) with corresponding X-ray elemental maps for Si, Ca, Al and S. **(B)** Close-up view of finer particles in the leach residue with corresponding Si, Ca, Al and S elemental maps.

(Queneau & Berthold, 1986). These monomers connect to each other through Si-O-Si branches to form a polysilicic acid and eventually colloids. Gelation occurs when these colloids connect to each other with entrapped liquid inside (Alkan et al., 2018), thus becoming unfilterable. The gelation rate is controlled by pH, the degree of supersaturation, temperature, the presence of seed particles, and salinity (Queneau & Berthold, 1986). The benefits of implementing hydrogen peroxide to bauxite residue leaching include have been mentioned to include dissolved Si precipitate as quartz without silica gel formation, formation of a titanium peroxosulfate complex yielding in a high Ti leaching efficiency and decreasing the amount of Sc-entrapping rhomboclase precipitation (Alkan et al., 2018). The formation of the orange complex occurred in all our experiments with H_2O_2, which is interpreted as the formation of titanium peroxosulfate, as described previously (Eq. 3 and 4). Leach residues of either the synthetic reference or Kiviniemi slags R1 and R3 after atmospheric leaching experiments did not indicate the presence of crystalline SiO_2 in the residues (Figure S2).

Amorphous material contains an extensive, irregular silicon-oxygen network, which would be expected to show only limited silica dissolution (Terry, 1983). On the other hand, amorphous material are generally expected to dissolve faster than its crystalline counterparts, with both showing increasing solubility with increasing temperature (Queneau & Berthold, 1986). Incongruent dissolution refers to preferential dissolution, which in practice means dissolution of cations over silica from either a crystalline or amorphous structure. In the case of crystalline structures, for silica to be present to any degree in solution, it must be present in the leaching material either as units of a small molecular weight or it must be broken into such units by the action of acid (Terry, 1983). Due to the strength of the Si-O-bonds, infinite silicate chains are not easily broken down into smaller silicate units, thus leaving a siliceous residue. However, this attribute is influenced, for example, by the alumina content of the silicate structure, as Al_2O_3 weakens the silicate network against acid attack. Furthermore, in any silicate material, the metal cation-oxygen bond is weaker than the silicon-oxygen bond and therefore more susceptible to acid attack – a semi-quantitative indication of the polarizing power of the metal cation is given by its ionic potential (ionic charge divided by ionic radius) (Terry, 1983). Similar features have been mentioned to apply to amorphous slag dissolution with the formation of a passive silica-enriched protective surface layer due to the preferential removal of metal ions (Fe, Mg, Al, Ca, K, Na) by acid (Perederiy and Papangelakis, 2017). This is consistent with the percolation model of glass dissolution (Cailletau et al., 2008), in which alkali and earth alkali cations are leached out, resulting in a siliceous layer. This is interpreted to occur in the synthetic reference and Kiviniemi R1 and R3 slags; the silica-enriched particles and layers are indications of preferential metal cation dissolution from an amorphous

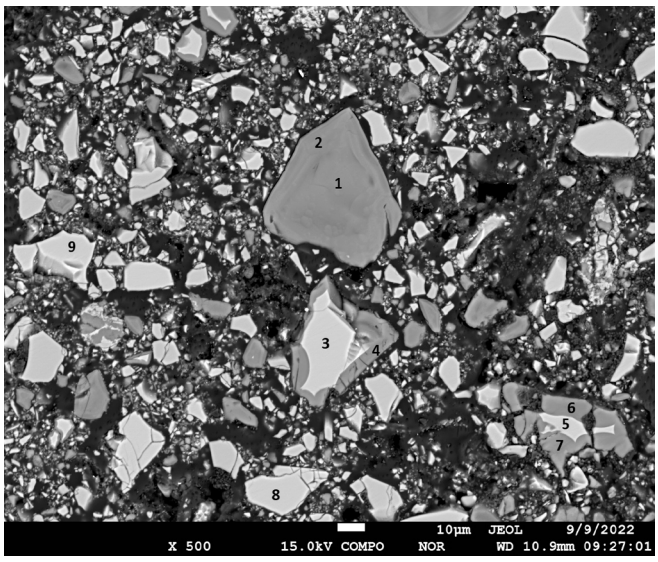

Fig. 9. (A) Back-scattered electron image of synthetic slag leach residue (2.5 M H_2O_2 + 2.5 M H_2SO_4, S/L 1:10, T = 100 °C), with the analysis points marked with numbers (analytical results listed in Table 4).

structure, with smaller slag particles responding easier to the acid, whereas larger particles exhibit intact interiors with silica-enriched outer layers on the slag particles. According to Perederiy and Papangelakis (2017), hydrolysis of the Si—O bonds leading to silica dissolution competes with re-polymerization of silica and precipitation of dissolved silicic acid along the path of the acid attack, thus precluding the complete dissolution.

It is often suggested that the properties Sc^{3+}(aq) in aqueous solutions are closer to those of Al^{3+} (ionic radius 54 pm) than to Y^{3+} (93 pm) or the lanthanide ions due to its smaller ionic radius (75 pm in octahedral coordination; Shannon, 1976). Scandium(III) functions as a hard metal ion (Pearson, 1963), although its complexes with fluoride and hydroxide are unusually strong in relation to its charge/radius ratio (Schrödle et al., 2008). Fig. 14 shows the distribution of Sc–hydroxide complexes as a function of pH and temperature (modified from Wood and Samson, 2006). At 25 °C, the hydrated Sc^{3+} ions predominate when pH is > 4 and at 100 °C, when pH is > 2. Increasing the temperature to 300 °C, all Sc species become hydrated, with Sc^{3+} being practically absent at all pH values.

Sc–sulfate complexes appear to be stronger than Sc–chloride complexes, but weaker than Sc–fluoride and –hydroxide complexes (Wood & Samson, 2006). In this study, HSC Chemistry 10 software was utilized to establish the Eh-pH diagram for Sc-S aqueous system at 50, 75 and 100 °C (Fig. 15). Based on the Eh-pH diagram, under the experimental conditions used, scandium exists as Sc^{3+}. With increasing temperature, Sc^{3+} stability area is slightly decreased towards lower acidity region.

3.4. High pressure acid leaching of synthetic and Kiviniemi R3 slag

Rivera et al. (2019) studied HPAL leaching of slags arising from the smelting of bauxite residue and reported up to 90 wt% of Sc extraction from crystalline slags using H_2SO_4 at 150 °C (SiO_2 10–26 wt%). According to their study, HPAL effectively suppressed the co-dissolution of silicon and titanium, particularly at temperatures above 100–120 °C. With respect to amorphous slag leaching, an extraction yield of ~ 85 wt % was documented. Therefore, a few HPAL experiments were conducted on the synthetic reference slag and the Kiviniemi R3 slag. Under the conditions applied in our study, leaching efficiencies appear similar with H_2O_2-assisted atmospheric H_2SO_4 leaching, although leaching efficiency of Sc for slag R3 is lower (~30 %) compared to ~ 40 % with atmospheric leaching (Fig. 16). Calcium is precipitated as anhydrite, as detected in XRD patterns (Figure S2). The titanium dissolution is somewhat suppressed in HPAL. The effects of pressure in the range studied in this work seem to be negligible to the leaching efficiency for the synthetic reference slag.

Table 4
Chemical compositions (wt%) determined by EPMA for particles of the synthetic slag leach residue. Analysis points (1–9) are shown Fig. 9.

Point	MgO	Al_2O_3	SiO_2	K_2O	CaO	S	Na_2O	Sc_2O_3	TiO_2	MnO	Total
1	0.00	0.45	61.39	0.22	10.19	4.96	0.11	0.03	0.47	0.02	85.32
2	0.08	1.34	75.56	0.06	0.06	2.64	0.01	0.03	0.35	0.03	84.14
3	1.83	18.53	53.96	1.52	15.35	0.01	1.02	1.12	4.27	1.11	98.82
4	0.02	0.84	73.81	0.13	0.17	0.62	0.01	0.02	0.50	0.03	77.08
5	1.51	16.46	50.31	1.22	14.61	0.01	0.75	1.08	4.12	0.98	91.14
6	0.05	0.21	39.18	0.02	0.12	0.37	0.01	0.02	0.60	0.04	41.20
7	0.01	0.13	46.77	0.11	0.24	0.44	0.02	0.02	0.45	0.03	48.91
8	1.80	17.51	56.77	1.39	14.93	0.01	0.96	1.07	3.73	0.99	99.22
9	1.69	16.94	57.17	1.60	14.55	0.02	1.02	1.00	3.26	1.03	98.38

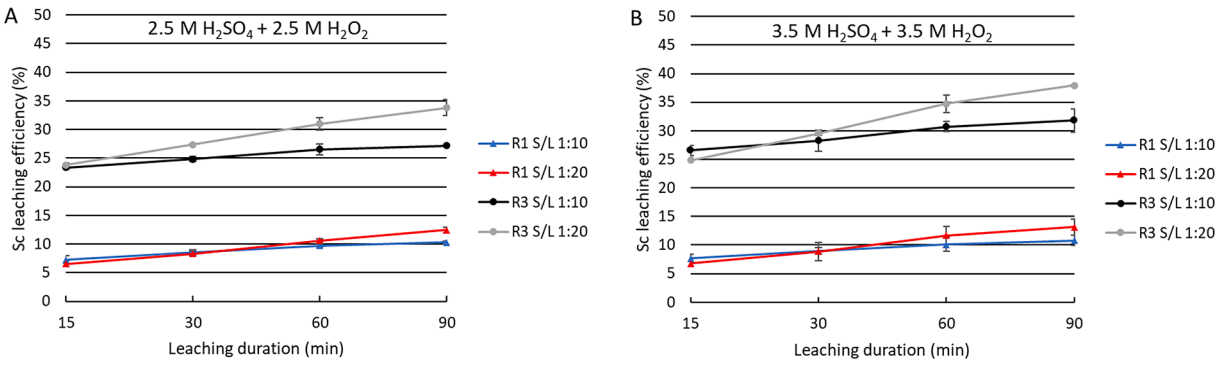

Fig. 10. Effects of H_2O_2 and H_2SO_4 molarity and S/L (1:10 and 1:20) on the Sc leaching efficiency for Kiviniemi slags R1 and R3. **(A)** 2.5 M H_2SO_4 + 2.5 M H_2O_2 **(B)** 3.5 M H_2SO_4 + 3.5 M H_2O_2. Temperature 100 °C. Error bars 2σ.

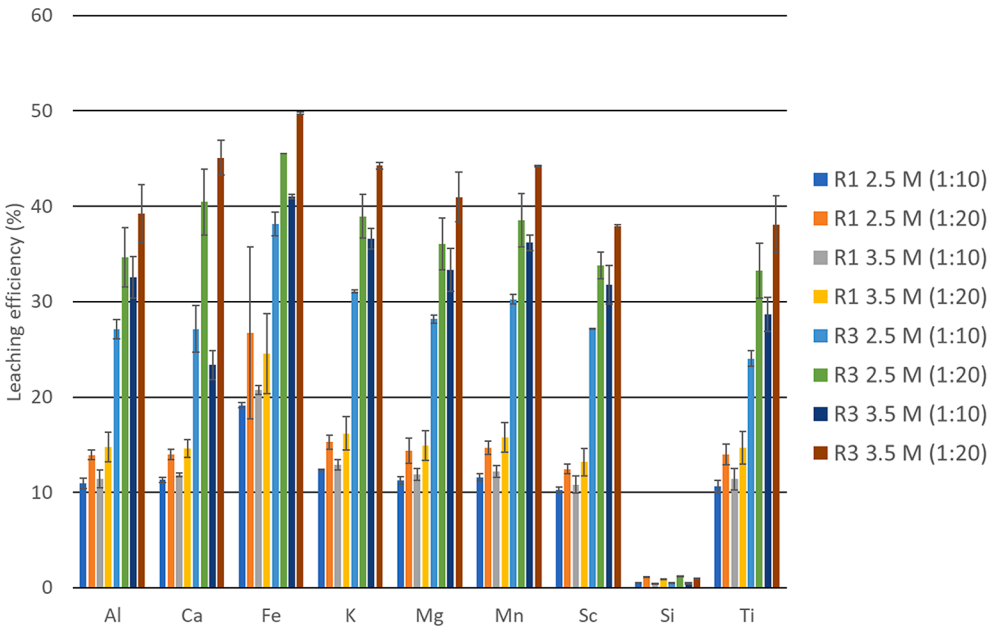

Fig. 11. Summary of average leaching efficiencies for Kiviniemi slags R1 and R3 with both tested molarities and S/L ratios (indicated in brackets) after 90 min leaching. Based on compositions of liquids determined by ICP-OES. Error bars 2σ.

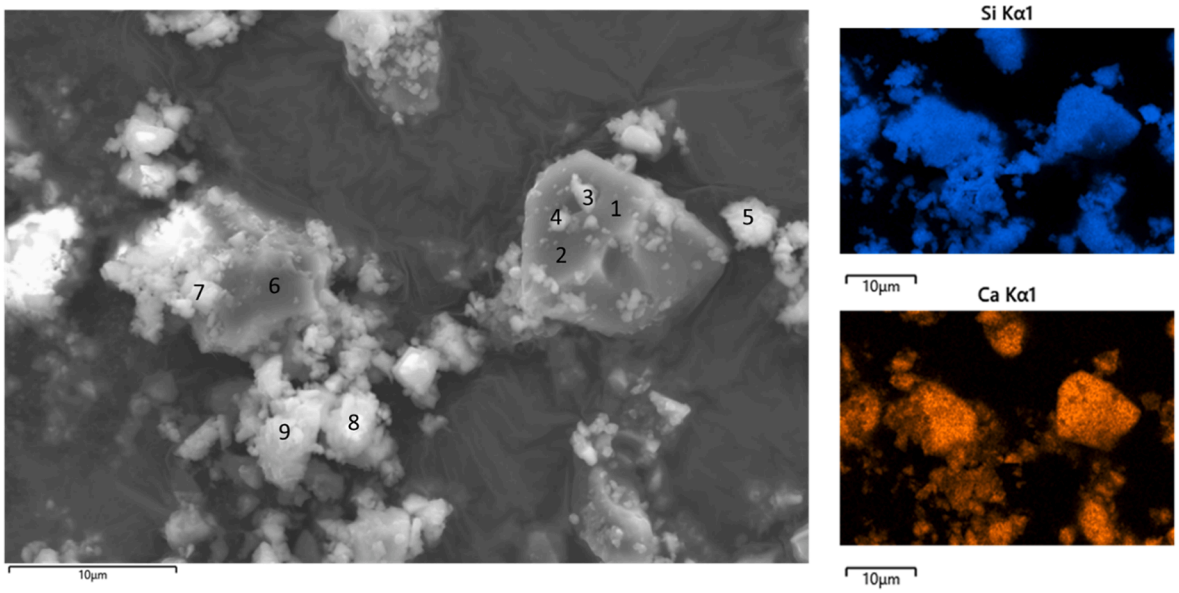

Fig. 12. Secondary electron image of slag R3 leach residue (2.5 M H_2O_2 + 2.5 M H_2SO_4 with S/L 1:20 at 100 °C) with corresponding X-ray elemental maps for Si and Ca.

Table 5
Chemical compositions of particles of slag R3 leach residue determined by FESEM-EDS. Analysis points (1–9) are shown in Fig. 12.

Point	MgO	Al_2O_3	SiO_2	K_2O	CaO	S	Na_2O	TiO_2	MnO	Total
1	1.77	16.89	66.75	2.05	18.78	0.60	2.10	3.25	0.66	112.85
2	1.76	15.87	62.90	2.05	18.54	0.54	1.71	3.15	0.58	107.10
3	1.39	12.74	65.33	1.41	13.50	1.02	1.62	2.45	0.50	99.97
4	1.26	12.41	67.97	1.40	12.40	1.23	1.87	2.35	0.40	101.29
5	0.00	5.67	79.45	0.22	3.48	0.25	0.00	1.27	0.00	90.34
6	1.43	14.25	59.86	1.94	18.04	0.45	1.44	3.22	0.68	101.30
7	0.00	8.67	73.91	0.93	8.35	0.99	0.81	1.85	0.00	95.52
8	0.71	8.71	72.52	0.00	7.60	0.27	0.00	1.67	0.00	91.48
9	0.83	10.05	76.67	0.00	9.18	0.26	0.00	2.12	0.00	99.11

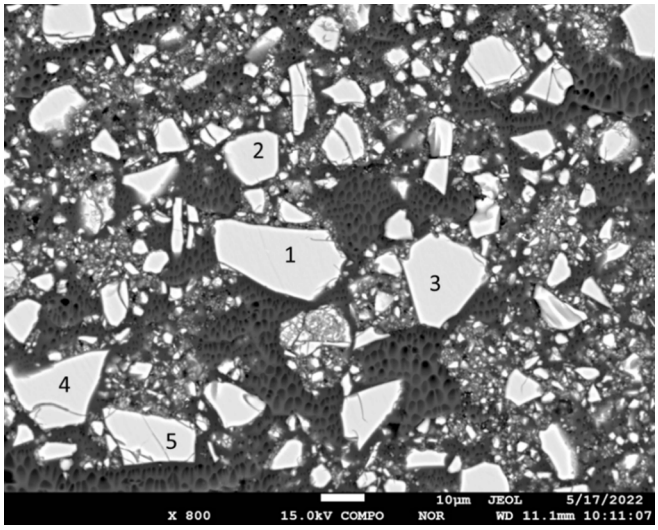

Fig. 13. Back-scattered electron image of slag R3 leach residue (2.5 M H_2O_2 + 2.5 M H_2SO_4 with S/L 1:20 at 100 °C) with analysis points marked by numbers.

4. Conclusions

The slags included in this study have extremely high silica contents (53–56 wt% SiO_2) compared to other materials investigated for the extraction of Sc, such as bauxite residues or slags derived from bauxite residue pyrometallurgical processing with SiO_2 contents up to 38 wt% SiO_2. Despite high SiO_2 content and amorphous structure, the Sc leaching efficiencies with H_2O_2-assisted H_2SO_4 leaching reached 40–50% for Kiviniemi R3 slag and synthetic reference slag, respectively. Considering other methods included in this study, Sc extraction with dry digestion was very limited, and leaching with HPAL remained at the level of 30–45 % under experimental conditions of 2.5 M H_2SO_4, 60 bar, and 150 °C. The high SiO_2 content of the slag is somewhat compensated by the small particle size for synthetic reference and Kiviniemi R3 slag, but the efficiency of leaching is negatively influenced by increased particle size with R1 slag. Observed siliceous particles and silica-enriched layers in leach residues indicate preferential metal cation dissolution from an amorphous structure, with smaller slag particles responding easier to the acid. Although silica gel formation under the applied conditions was avoided, further studies should be conducted to improve leaching efficiencies with respect to Sc extraction. These could include controlled cooling of the slag to produce crystalline structures and to investigate the possibility of selective leaching, considering also further adjustment of slag chemical composition. Furthermore, future aspects of processing Kiviniemi concentrates could include hydrogen-based reduction to minimize the carbon footprint of the suggested processing scenario.

Funding: This research has been funded by the K.H. Renlund Foundation and The Foundation for Research of Natural Resources in Finland, grant number 20210019.

CRediT authorship contribution statement

Rita Kallio: Conceptualization, Methodology, Investigation, Writing – original draft, Visualization. **Ulla Lassi:** Conceptualization, Methodology, Resources, Supervision. **Toni Kauppinen:** Visualization, Conceptualization, Methodology. **Eveliina Holappa:** Methodology, Investigation. **Mika Christophliemk:** Methodology, Investigation. **Saija Luukkanen:** Supervision, Resources, Writing – review & editing. **Pekka Tanskanen:** Supervision, Writing – review & editing. **Timo Fabritius:** Supervision, Resources, Writing – review & editing, Project

Table 6
Chemical compositions (wt%) of particles of slag R3 leach residue determined by EPMA. Analysis points (1–5) are shown Fig. 13.

Point	MgO	Al_2O_3	SiO_2	K_2O	CaO	S	Na_2O	Sc_2O_3	TiO_2	MnO	Total
1	1.45	14.01	55.97	2.20	19.67	0.28	1.60	0.05	3.51	0.64	99.98
2	1.45	14.14	55.80	2.17	19.79	0.29	1.64	0.05	3.50	0.69	100.11
3	1.41	14.09	56.08	2.17	19.66	0.29	1.63	0.05	3.55	0.69	100.19
4	1.44	14.07	56.13	2.19	19.66	0.30	1.67	0.06	3.54	0.61	100.24
5	1.42	13.77	55.60	2.17	19.79	0.27	1.67	0.06	3.38	0.59	99.23

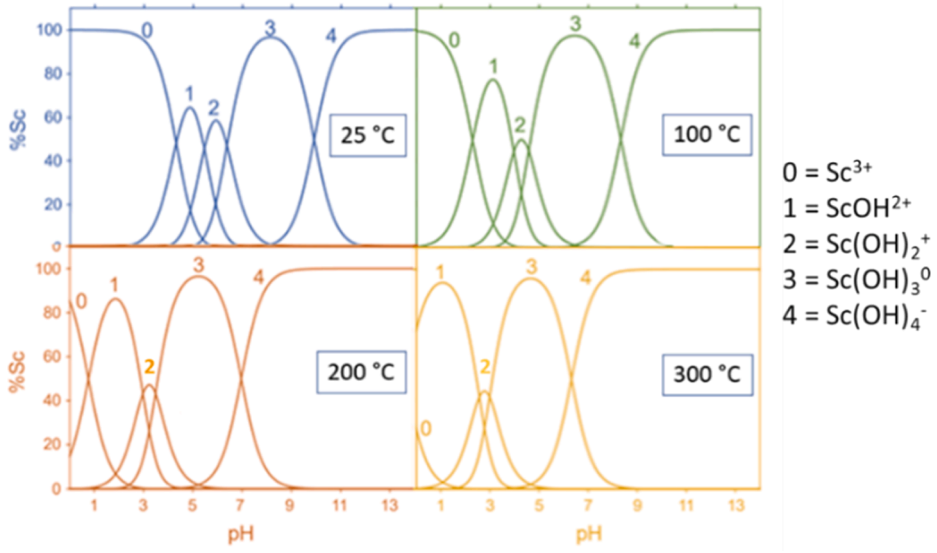

Fig. 14. Distribution of Sc^{3+} hydroxide complexes as a function of pH at 25, 100, 200 and 300 °C at saturated water vapor pressure (adapted from Wood and Samson, 2006, with the permission from Elsevier).

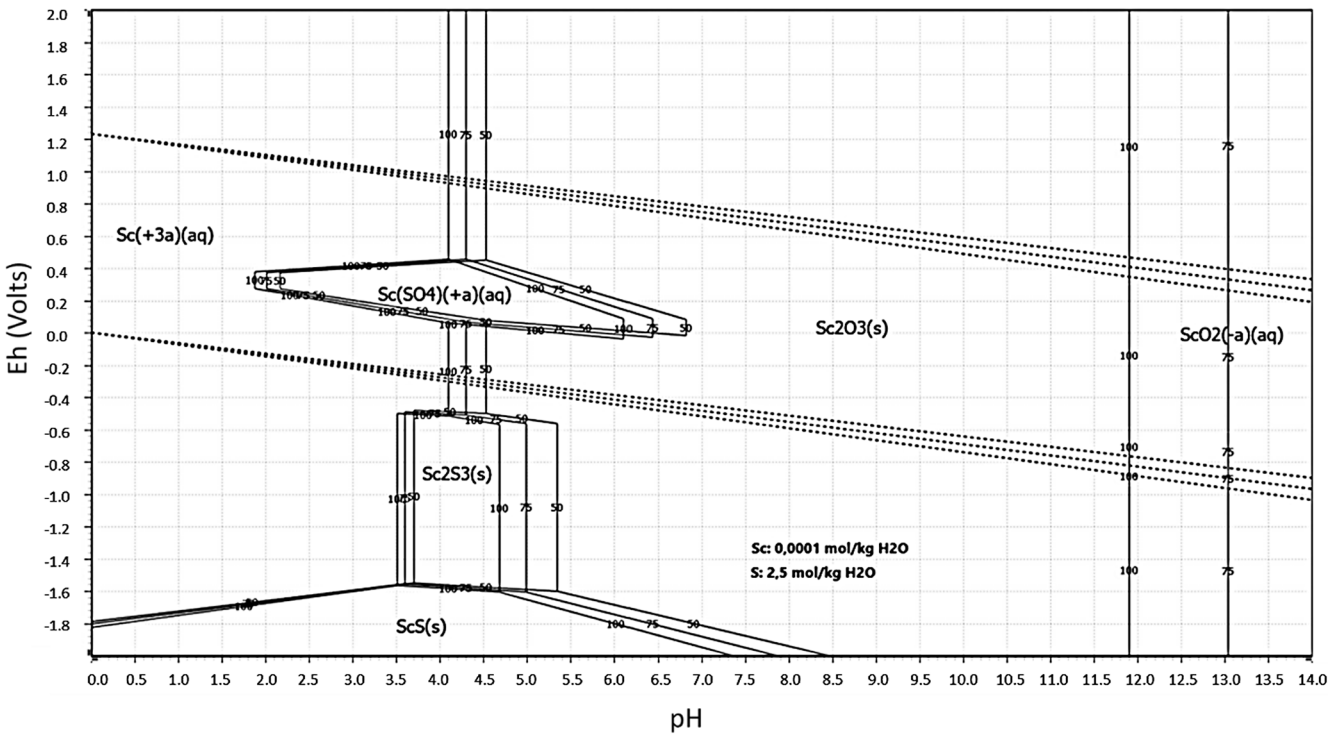

Fig. 15. Eh-pH diagram for the Sc-S aqueous system at 50, 75 and 100 °C. Constructed using HSC Chemistry 10 software.

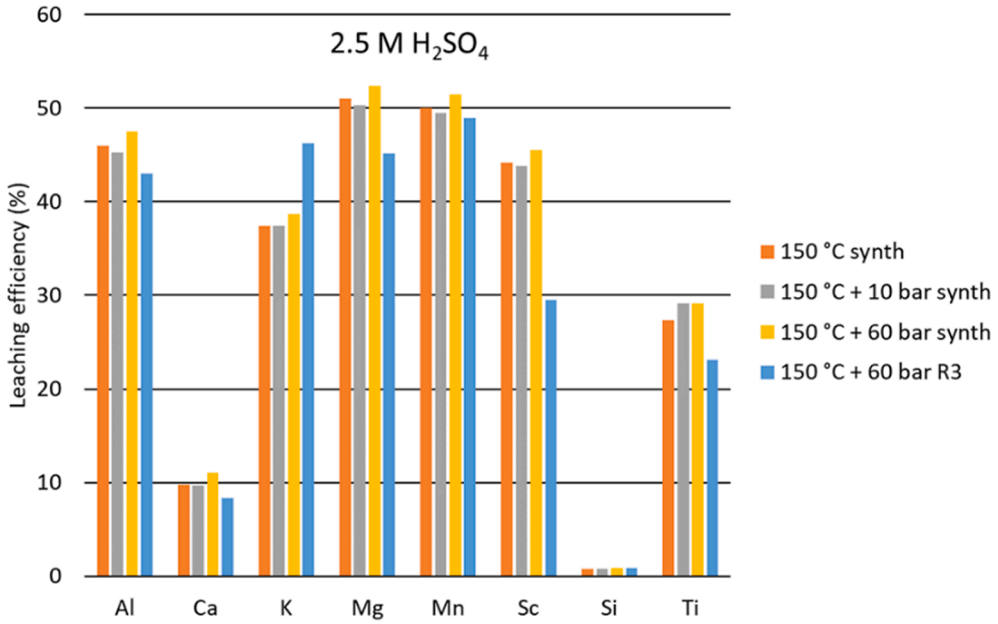

Fig. 16. Summary of the leaching efficiencies for the synthetic slag (synth) and Kiviniemi R3 slag with 2.5 M H_2SO_4 HPAL experiments as based on liquid compositions determined by ICP-OES.

administration.

Declaration of Competing Interest

The authors declare that they have no known competing financial interests or personal relationships that could have appeared to influence the work reported in this paper.

Data availability

Data will be made available on request.

Acknowledgments

Support and advice from the doctoral training follow-up group members, Jussi Liipo and Tapio Halkoaho, are highly appreciated. The samples from Kiviniemi were provided by GTK, and Metso Outotec enabled the experiments with LIMS and SLon, which are all gratefully

acknowledged. The authors are also thankful to Eero Hanski for comments on the manuscript.

Appendix A. Supplementary data

Supplementary data to this article can be found online at https://doi.org/10.1016/j.mineng.2022.107901.

References

Ahmad, Z., 2003. The properties and application of scandium-reinforced aluminium. J. MineralsMetals Mater. Soc. (TMS) 55 (2), 35–39.

Alkan, G., Schier, C., Gronen, L., Stopic, S., Friedrich, B., 2017. A mineralogical assessment on residues after acidic leaching of bauxite residue (Red mud) for titanium recovery. Metals 7 (11). https://doi.org/10.3390/met7110458.

Alkan, G., Yagmurlu, B., Cakmakoglu, S., Hertel, T., Kaya, Ş., Gronen, L., Stopic, S., Friedrich, B., 2018. Novel approach for enhanced scandium and titanium leaching efficiency from bauxite residue with suppressed silica gel formation. Sci. Rep. 8 (1), 1–12. https://doi.org/10.1038/s41598-018-24077-9.

Alkan, G., Yagmurlu, B., Gronen, L., Dittrich, C., Ma, Y., Stopic, S., Friedrich, B., 2019. Selective silica gel free scandium extraction from iron-depleted red mud slags by dry digestion. Hydrometallurgy 185 (March), 266–272. https://doi.org/10.1016/j.hydromet.2019.03.008.

Anawati, J., Azimi, G., 2022. Integrated carbothermic smelting – acid baking – water leaching process for extraction of scandium, aluminum, and iron from bauxite residue. J. Cleaner Prod. 330 (November 2021), 129905 https://doi.org/10.1016/j.jclepro.2021.129905.

Bisaka, K., Thobadi, I.C., Pawlik, C., 2017. Extraction of rare earths from iron-rich rare earth deposits. J. South Afr. Inst. Min. Metall. 117 (8), 731–739. https://doi.org/10.17159/2411-9717/2017/v117n8a2.

Blengini, G., El Latunussa, C., Eynard, U., et al., 2020. Study on the EU's list of critical raw materials (2020): critical raw materials factsheets.. https://data.europa.eu/doi/10.2873/92480 (Accessed 06 September 2021).

Borra, C.R., Pontikes, Y., Binnemans, K., Van Gerven, T., 2015. Leaching of rare earths from bauxite residue (red mud). Minerals Engineering 76, 20–27. https://doi.org/10.1016/j.mineng.2015.01.005.

Botelho Junior, A.B., Espinosa, D.C.R., Vaughan, J., Tenório, J.A.S., 2021. Recovery of scandium from various sources: A critical review of the state of the art and future prospects. Miner. Eng. 172 (May), 1–20. https://doi.org/10.1016/j.mineng.2021.107148.

Bueno, M., Torvela, J., Chandramohan, R., Chavez Matus, T., Liedes, T., Powell, M., 2021. The double wheel breakage test. Miner. Eng. 168 (June 2020), 106905 https://doi.org/10.1016/j.mineng.2021.106905.

Cailletau, C., Weigel, C., Ledieu, A., Barboux, P., Devreus, F., 2008. On the effect of glass composition in the dissolution of glasses by water. Journal of Non-Crystalline Sollids 354, 117–123. https://doi.org/10.1016/j.jnoncrysol.2007.07.063.

Connelly, N.G., Hartshorn, R.M., Damhus, T., Hutton, A.T., 2005. Nomenclature of inorganic chemistry IUPAC recommendations 2005. Royal Society of Chemistry Vol. 128, Issue 21.

Duyvesteyn, W., & Putnam, G. (2014). *Scandium, a review of the element, its characteristics, and current and emerging commercial applications [White paper]*.

Eilu, P. (2017). Critical raw materials factsheets. *European Commision*, *June*, 515. https://doi.org/10.2873/398823.

Fan, H.R., Yang, K.F., Hu, F.F., Liu, S., Wang, K.Y., 2016. The giant Bayan Obo REE-Nb-Fe deposit, China: Controversy and ore genesis. Geosci. Front. 7 (3), 335–344. https://doi.org/10.1016/j.gsf.2015.11.005.

Faris, N., Ram, R., Tardio, J., Bhargava, S., McMaster, S., Pownceby, M.I., 2017. Application of ferrous pyrometallurgy to the beneficiation of rare earth bearing iron ores – A review. Miner. Eng. 110 (February), 20–30. https://doi.org/10.1016/j.mineng.2017.04.005.

Gorrepati, E.A., Wongthahan, P., Raha, S., Fogler, H.S., 2010. Silica precipitation in acidic solutions: mechanism, pH effect, and salt effect. Langmuir 26 (14), 10467–10474. https://doi.org/10.1021/la904685x.

Gupta, G.K., Krishnamurthy, N., 2005. Extractive metallurgy of rare earths. In: Extractive metallurgy of rare earths, Vol. 37, Issue 1. CRC Press. https://doi.org/10.1179/imr.1992.37.1.197.

Halkoaho, T., Ahven, M., Rämö, O. T., Hokka, J., & Huhma, H. (2020). Petrography, geochemistry and geochronoloy of the Sc-enriched Kiviniemi ferrodiorite intrusion, eastern Finland. *Mineralium Deposita*, 1–20. https://doi.org/https://doi.org/10.1007/s00126-020-00952-2.

Hokka, J., & Halkoaho, T. (2016). *3D modelling and mineral resource estimation of the Kiviniemi Scandium deposit, Eastern Finland* (Issue January). https://doi.org/10.13140/RG.2.2.25709.18400.

Halkoaho, T., Niskanen, M., 2015. A research report of scandium and zirconium studies concerning the claim area of Kiviniemi 1 (register number of claim: 8777/1) in Rautalampi area during years 2008-2010 (in finnish). Claim report, Geological Survey of Finland 56, 1–32.

Jordens, A., Cheng, Y.P., Waters, K.E., 2013. A review of the beneficiation of rare earth element bearing minerals. Minerals Engineering 41, 97–114. https://doi.org/10.1016/j.mineng.2012.10.017.

Kallio, R., Tanskanen, P., Heikkinen, E.P., Kokkonen, T., Luukkanen, S., Fabritius, T., 2022a. Reduction characteristics of Kiviniemi ferrous scandium concentrate. Miner. Eng. 177 (October 2021), 107369 https://doi.org/10.1016/j.mineng.2021.107369.

Kallio, R., Tanskanen, P., Heikkinen, E.P., Kokkonen, T., Luukkanen, S., Fabritius, T., 2022b. Slag modification in reduction of Kiviniemi ferrous scandiun concentrates. Metals 12 (709). https://doi.org/10.3390/met12050709.

Kallio, R., Tanskanen, P., Luukkanen, S., 2021. Magnetic preconcentration and process mineralogical study of the Kiviniemi Sc-enriched ferrodiorite, eastern Finland. Minerals 11 (966). https://doi.org/10.3390/min11090966.

Kim, J., Azimi, G., 2020. Recovery of scandium and neodymium from blast furnace slag using acid baking-water leaching. RSC Adv. 10 (53), 31936–31946. https://doi.org/10.1039/d0ra05797e.

Li, G., Liu, M., Rao, M., Jiang, T., Zhuang, J., Zhang, Y., 2014. Stepwise extraction of valuable components from red mud based on reductive roasting with sodium salts. J. Hazard. Mater. 280, 774–780. https://doi.org/10.1016/j.jhazmat.2014.09.005.

Li, Y., Papangelakis, V.G., Perederiy, I., 2009. High pressure oxidative acid leaching of nickel smelter slag: Characterization of feed and residue. Hydrometallurgy 97 (3–4), 185–193. https://doi.org/10.1016/j.hydromet.2009.03.007.

Pearson, R.G., 1963. Hard and soft acids and bases. J. Am. Chem. Soc. 85 (22), 3533–3539.

Perederiy, I., 2011. Dissolution of valuable metals from nickel smelter slags by means of high pressure oxidative acid leaching. University of Toronto, p. 122 p.. Dissertation,.

Perederiy, I., Papangelakis, V.G., 2017. Why amorphous FeO-SiO2 slags do not acid-leach at high temperatures. J. Hazard. Mater. 321, 737–744. https://doi.org/10.1016/j.jhazmat.2016.09.055.

Queneau, P.B., Berthold, C.E., 1986. Silica in hydrometallurgy: An overview. Can. Metall. Q. 25 (3), 201–209. https://doi.org/10.1179/000844386795430270.

Rivera, R.M., Ulenaers, B., Ounoughene, G., Binnemans, K., Van Gerven, T., 2018. Extraction of rare earths from bauxite residue (red mud) by dry digestion followed by water leaching. Miner. Eng. 119 (February), 82–92. https://doi.org/10.1016/j.mineng.2018.01.023.

Rivera, R.M., Xakalashe, B., Ounoughene, G., Binnemans, K., Friedrich, B., Van Gerven, T., 2019. Selective rare earth element extraction using high-pressure acid leaching of slags arising from the smelting of bauxite residue. Hydrometallurgy 184 (December 2018), 162–174. https://doi.org/10.1016/j.hydromet.2019.01.005.

Schrödle, S., Wachter, W., Buchner, R., Hefter, G., 2008. Scandium sulfate complexation in aqueous solution by dielectric relaxation spectroscopy. Inorg. Chem. 47 (19), 8619–8628. https://doi.org/10.1021/ic702396r.

Shannon, R.D., 1976. Revised effective ionic radii and systematic studies of interatomic distances in halides and chalcogenides. Acta Crystallographica Section A 32 (5), 751–767. https://doi.org/10.1107/S0567739476001551.

Terry, B., 1983. The acid decomposition of silicate minerals part I. Reactivities and modes of dissolution of silicates. Hydrometallurgy 10 (2), 135–150.

U.S.G.S. (2022). *Mineral commodity summaries 2022*. https://pubs.usgs.gov/periodicals/mcs2022/mcs2022-zeolites.pdf.

Voßenkaul, D., Birich, A., Müller, N., Stoltz, N., Friedrich, B., 2017. Hydrometallurgical processing of eudialyte bearing concentrates to recover rare earth elements via low-temperature dry digestion to prevent the silica gel formation. Journal of Sustainable Metallurgy 3 (1), 79–89. https://doi.org/10.1007/s40831-016-0084-2.

Wang, W., Pranolo, Y., Cheng, C.Y., 2011. Metallurgical processes for scandium recovery from various resources: A review. Hydrometallurgy 108 (1–2), 100–108. https://doi.org/10.1016/j.hydromet.2011.03.001.

Williams-Jones, A.E., Vasyukova, O.V., 2018. The economic geology of scandium, the runt of the rare earth element litter. Econ. Geol. 113 (4), 973–988. https://doi.org/10.5382/econgeo.2018.4579.

Wood, S.A., Samson, I.M., 2006. The aqueous geochemistry of gallium, germanium, indium and scandium. Ore Geol. Rev. 28 (1), 57–102. https://doi.org/10.1016/j.oregeorev.2003.06.002.

Yagmurlu, B., Alkan, G., Xakalashe, B., Schier, C., Gronen, L., Koiwa, I., Dittrich, C., Friedrich, B., 2019. Synthesis of scandium phosphate after peroxide assisted leaching of iron depleted bauxite residue (red mud) slags. Sci. Rep. 9 (1), 1–10. https://doi.org/10.1038/s41598-019-48390-z.

Yagmurlu, B., Zhang, W., Avdibegovic, D., Regadío, M., Koivula, R., Dittrich, C., Binnemans, K., & Friedrich, B. (2018). Advances on scandium recovery beyond state of the art. *ALTA 2018 Uranium-REE-Lithium Proceedings*, *July*, 85–93.

Zakaria, Z., Kamarudin, S.K., 2021. Advanced modification of scandia-stabilized zirconia electrolytes for solid oxide fuel cells application—A review. Int. J. Energy Res. 45 (4), 4871–4887. https://doi.org/10.1002/er.6206.

Zhou, K., Teng, C., Zhang, X., Peng, C., Chen, W., 2018. Enhanced selective leaching of scandium from red mud. Hydrometallurgy 182 (March), 57–63. https://doi.org/10.1016/j.hydromet.2018.10.011.

Zhou, Y., Yang, H., Xue, X., Yuan, S., 2017. Separation and recovery of iron and rare earth from Bayan Obo tailings by magnetizing roasting and (NH4)2SO4 activation roasting. Metals 7 (6), 195. https://doi.org/10.3390/met7060195.